Microelectronic Engineering 85 (2008) 1647–1651

Contents lists available at ScienceDirect

Microelectronic Engineering

journal homepage: www.elsevier.com/locate/mee

Fabrication and electrical characteristics of Schottky diode based on organic material

Ö. Güllü *, Ş. Aydoğan, A. Türüt

Atatürk University, Faculty of Sciences and Arts, Department of Physics, 25240 Erzurum, Turkey

ARTICLE INFO

Article history:
Received 8 December 2007
Received in revised form 1 March 2008
Accepted 3 April 2008
Available online 12 April 2008

Keywords:
Schottky diode
Barrier height
Ideality factor
Series resistance
Orange G

ABSTRACT

The current–voltage (*I–V*), capacitance–voltage (*C–V*) and capacitance–frequency (*C–f*) characteristics of Al/Orange G/*n*-Si/AuSb structure were investigated at room temperature. A modified Norde's function combined with conventional forward *I–V* method was used to extract the parameters including barrier height (BH) and the series resistance. The barrier height and series resistance obtained from Norde's function was compared with those from Cheung functions, and it was seen that there was a good agreement between series resistances from both methods. The *C–V* characteristics were performed at 10 kHz and 500 kHz frequencies, and *C–f* characteristics were performed 0.0 V, +0.4 V and −0.4 V.

1. Introduction

Considerable attention was given in recent years to the fabrication and characterization of Schottky diodes organic light emitting diodes, organic field effect transistors, photovoltaic (PV) and solar cells, using organic semiconductors and their derivatives, due to their stability and barrier height enhancement properties [1–7]. Furthermore, more recently, electronic systems are moving to the ultimate scale of molecular entities, as demonstrated by the growing interest in understanding transport through organic molecules bridging two metal contacts [8,9] and metal/organic material/semiconductor structure [10–13]. Schottky diodes made by introducing a thin aniline green and methyl violet organic layer on Si based structures have been shown to exhibit promising characteristics for diode applications [12,13]. Among those, Orange G (OG) is considered to be a good candidate for organic semiconductor devices fabrication such as Schottky device and solar cell. Because, it offers a possibility of low-cost and large-area devices. OG have also attracted the researchers attentions due to their easiness of synthesis, good environmental stability and high degree response of humidity, but unfortunately a little amount of information is available in scientific literature about electrical properties of OG [7]. OG with molecular formula $C_{16}H_{10}N_2O_7S_2Na_2$ (1,3-naphthalenedisulfonic acid, 7-hydroxy-8-(phenylazo)-, disodium salt) used in this study is a typical aromatic azo compound. The molecular structure of the OG is given in Fig. 1. The structure of azo dyes has attracted considerable attentions recently due to their wide applicability in the light-induced photo isomerization process, and their potential usage for the reversible optical data storage [12].

Organic/inorganic semiconductor structures or metal/semiconductor (MS) contacts [14] are of great importance since they are present in most semiconductor device. It is well known that the interfacial properties of these contacts have a dominant influence on device performance, reliability and stability. There is a native thin insulating layer of oxide on the surface of the semiconductor in most practical MS contacts. This layer converts the MS structure into a metal/insulator/semiconductor device [15]. Besides, it can be constructed as an organic thin film between metal and semiconductor intentionally. This film modifies some characteristics of devices. Because, Schottky barrier heights of MS contacts can be manipulated by insertion of a dipole layer between the semiconductor and the organic film. So far many attempts have been made to realize a modification and the continuous control of the barrier height using an organic semiconducting layer, an insulating layer and/or a chemical passivation procedure at certain metal/inorganic semiconductor interfaces, or to determine characteristic parameters of organic film [16–28]. Campbell et al. [16] have used organic thin film to introduce a controlled dipole layer at the semiconductor/organic interface and thus change the effective Schottky barrier height. They reported that the effective Schottky barrier could be either increased or decreased by using organic thin layer on inorganic semiconductor. Also, thicker organic interlayers of the conjugated molecules have also been successfully used to modify effective barriers [23–27].

* Corresponding author. Tel.: +90 442 231 4081; fax: +90 442 236 0948.
E-mail address: omergullu@gmail.com (Ö. Güllü).

0167-9317/$ - see front matter © 2008 Elsevier B.V. All rights reserved.
doi:10.1016/j.mee.2008.04.003

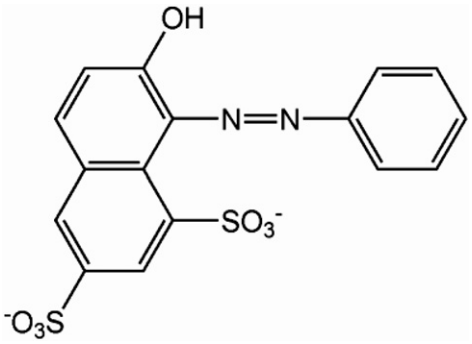

Fig. 1. Chemical structure of Orange G (OG).

Our purpose is to fabricate a Al/OG/*n*-Si/AuSb and to study the suitability and possibility of organic-on inorganic semiconductor contacts for use in barrier modification of Si metal/semiconductor diode. For this purpose, we investigate some junction parameters of the structure by the electrical measurements such as; current–voltage, capacitance–voltage and capacitance–frequency.

2. Experimental details

In this study, phosphorus (P) doped *n*-type Si wafer with (1 0 0) orientation, 400 μm thickness, 1–10 Ω-cm resistivity and a doping concentration of 5×10^{17} cm^{-3} from the *C*–*V* measurement was used and then, the *n*-Si wafer was chemically cleaned using the RCA cleaning procedure (i.e. 10 min boil in $NH_3 + H_2O_2 + 6H_2O$ followed by a 10 min $HCl + H_2O_2 + 6H_2O$ at 60 °C) before making contacts. The ohmic contact was made by evaporating AuSb alloy on the back of the substrate then, was annealed at 420 °C for 3 min in N_2 atmosphere. The native oxide on the front surface of the *n*-Si substrate was removed in $HF + 10H_2O$ solution. Finally, it was rinsed in de-ionized water for 30 s and was dried in N_2 atmosphere before forming an organic layer on the *n*-type Si substrate. OG organic layer was directly formed by adding 4 μL of the Orange G organic compound solution (wt 0.2% in ethanol) obtained from OG purchased by Merck firm (Merck Cat. No. 1.15925, Orange G, not specified its purity) on the front surface of the *n*-Si wafer, and was dried by itself the solvent in N_2 atmosphere for one hour. The thickness of the OG film was calculated as 65 nm from the high frequency *C*–*V* characteristics ($C = \varepsilon_s A/d$, where *C* is the capacitance in 500 kHz. Then, to perform the electrical measurements Al was evaporated on the OG at 10^{-5} torr (the diode diameter is 1 mm). In this way the Al/OG/*n*-Si/AuSb structure was obtained. A schematic cross-section of the Al/OG/*n*-Si/AuSb structure is shown in Fig. 2. The *I*–*V* and *C*–*V*–*f* measurements of this structure were performed with KEITLEY 487 Picoammeter/Voltage Source and HP 4192A (50 Hz-13 MHz) LF IMPEDENCE ANALYZER, respectively.

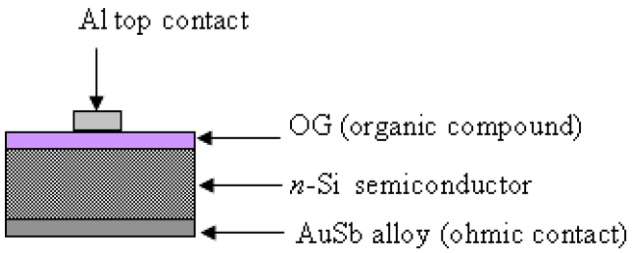

Fig. 2. A schematic cross-section of the Al/OG/*n*-Si/AuSb structure.

3. Results and discussion

According to the thermionic emission (TE) theory, the current in Schottky barrier diodes (SBDs) can be expressed as [15]:

$$I = AA^*T^2 \exp\left(-\frac{q\Phi_b}{kT}\right)\left[\exp\left(\frac{qV}{nkT}\right) - 1\right] \quad (1)$$

where

$$I_0 = AA^*T^2 \exp\left(-\frac{q\Phi_b}{kT}\right) \quad (2)$$

is the saturation current, Φb is the effective barrier height at zero-bias, A^* is the Richardson constant and equals to 112 A/cm2K2 for *n*-type Si, where *q* is the electron charge, *V* is the forward bias voltage, *A* is the effective diode area, *k* is the Boltzmann's constant, *T* is the temperature in Kelvin, *n* is the ideality factor, and it is determined from the slope of the linear region of the forward bias ln *I*–*V* characteristic through the relation:

$$n = \frac{q}{kT}\frac{dV}{d(\ln I)}. \quad (3)$$

n equals to one for an ideal diode. However, *n* has usually a value greater than unity. High values of *n* can be attributed to the presence of native oxide layer and a wide distribution of low-SBH patches (or barrier inhomogeneities), and therefore, to the bias voltage dependence of the SBH [15,28,29].

Φ_b is the zero-bias barrier height (BH), which can be obtained from the following equation:

$$\Phi_b = kT/q \ln(AA^*T^2/I_0) \quad (4)$$

Fig. 3 represents the forward bias current–voltage (*I*–*V*) characteristics of the Al/OG/*n*-Si/AuSb structure. The values of the *n* and Φ_b obtained from *I*–*V* characteristics using Eqs. (3) and (4) are 4.35 and 0.86 eV, respectively. The high values in the ideality factor are caused possibly by other effects, such as organic layer effect, inhomogeneities of organic film thickness, etc. In order to find out ohmicity of Al it has also been investigated the *I*–*V* characteristic of an Al/OG/Al contact shown in the inset of Fig. 3. This figure shows that there is an ohmic behavior between the Al and the OG layer.

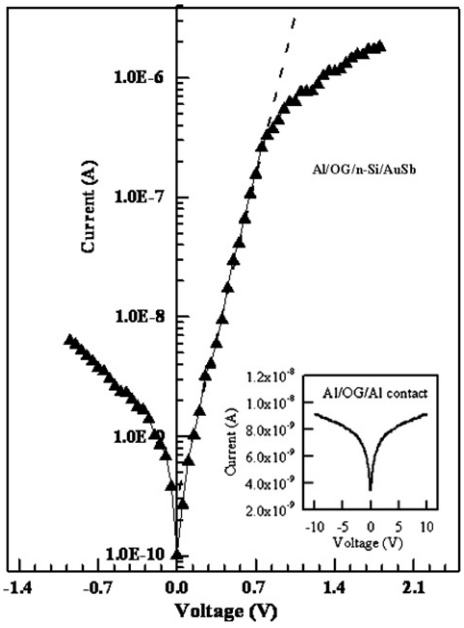

Fig. 3. The current–voltage characteristics of the Al/OG/*n*-Si/AuSb structure. Inset depicts the ohmicity of Al and OG layer.

Furthermore, to understand which mechanisms can control the diode behavior the *I–V* characteristic of the Al/OG/*n*-Si device is presented in log–log scale in Fig. 4. This suggests that the conduction processes occurring in the quercetin film of the Al/OG/*n*-Si device would be a possible alternative candidate in determining the forward current at the intermediate and high bias voltage [30]. As can be also seen from the double logarithmic forward bias *I–V* plot in Fig. 4, the charge transport is mainly governed by space-charge-limited current (SCLC) process. That is, the double logarithmic forward bias *I–V* plot shows a power law behavior of the current $I \propto V^{m+1}$ with different exponents $(m+1)$. Thus, the transport through the OG organic film is governed by the trapped-charge-limited current (TCLC) in the band gap of the organic layer [30–33]. That is, the SCLC conduction should become important when the density of injected free-charge carriers is much larger than the thermal-generated free-charge-carrier density.

In the present case, as can be also seen from the log*I*–log*V* plot in Fig. 4, the injected charge carriers can be proceed through the junction from the n-Si into the OG material with much lower concentration. As can be seen from Fig. 4, the forward bias characteristics show three linear regions separated by transition segments. The region I shows an ohmic region with a slope of one up to a transition voltage of about 0.2 V which obeys the current expression $J = q\mu n_0 V/d$, where n_0 is the concentration of the free carriers in the organic layer, μ is the carrier mobility in organic layer and d is the thickness of the organic layer. When considering the Al/OG/*n*-Si structure, the region II of the forward bias characteristic having a slope of 5 for $(m+1)$ is very similar to that of the SCLC with an exponential distribution of traps in the band gap of the organic material, that is, this model implies that the TCL currents dominate in the organic semiconductor OG at high injection. The slope of the region III in the double logarithmic forward bias characteristic of the device has a value of 2 for the Al/OG/*n*-Si. As can be seen, at high voltages the slope of the plot tends to decrease because the device approaches the 'trap-filled' limit when the injection level is high whose dependence is the same as in the trap-free space-charge-limited current [30–33].

It is well known that the downward concave curvature of the forward bias current–voltage plots at sufficiently large voltages is caused by the presence of the effect of R_s, apart from the interface states, which are in equilibrium with the semiconductor [34]. If the series resistance effect is low, the non-linear region will be narrow [35]. The values of the R_s were calculated using a method developed by Cheung and Cheung [36]. According to Cheung and Cheung [36], the forward bias *I–V* characteristics due to the TE of a Schottky diode with the series resistance can be expressed as,

$$I = I_0 \exp\left[\frac{q(V - IR_s)}{nkT}\right], \tag{5}$$

where the IR_s term is the voltage drop across series resistance of device. The values of the series resistance can determined from following function using Eq. (5):

$$\frac{dV}{d(\ln I)} = \frac{nkT}{q} + IR_s, \tag{6}$$

$$H(I) = V - \left(\frac{nkT}{q}\right)\ln\left(\frac{I}{AA^*T^2}\right), \tag{7}$$

and $H(I)$is given as follows:

$$H(I) = n\Phi_b + IR_s, \tag{8}$$

A plot of $\frac{dV}{d(\ln I)}$ *vs. I* will be linear and gives R_s as the slope and $\frac{nkT}{q}$ as the *y*-axis intercept from Eq. (6). Fig. 5 shows a plot of $\frac{dV}{d(\ln I)}$ *vs. I* at room temperature. The values of n and R_s have been calculated as $n = 4.19$ and $R_s = 398.8\ \text{k}\Omega$, respectively. It has been observed that there is a small difference between the values of n obtained from the forward bias ln*I–V* plot and from the d*V*/d(ln*I*)–*I* curves. This may be attributed to the existence of the series resistance and interface states, and to the voltage drop across the interfacial layer [37].

Besides, *H(I) vs. I* will be linear, the slope of this plot provides a different determination of R_s. Thus, by using the value of the n obtained from Eq. (6) the value of Φ_b can be calculated from the *y*-axis intercept of the *H*(*I*)–*I* plot. The *H(I) vs. I* is shown in Fig. 5 too. From *H*(*I*) *vs. I* plot, Φ_b and R_s were calculated as 0.84 eV and 306.8 kΩ, respectively.

Furthermore, Norde proposed an alternative method to determine value of the series resistance. The following function has been defined in the modified Norde's method [38,39]:

$$F(V) = \frac{V}{\gamma} - \frac{kT}{q}\ln\left(\frac{I(V)}{AA^*T^2}\right) \tag{9}$$

where γ is the first integer (dimensionless) greater than n. Here it has been taken as 5. The $I(V)$ is current obtained from the *I–V* curve.

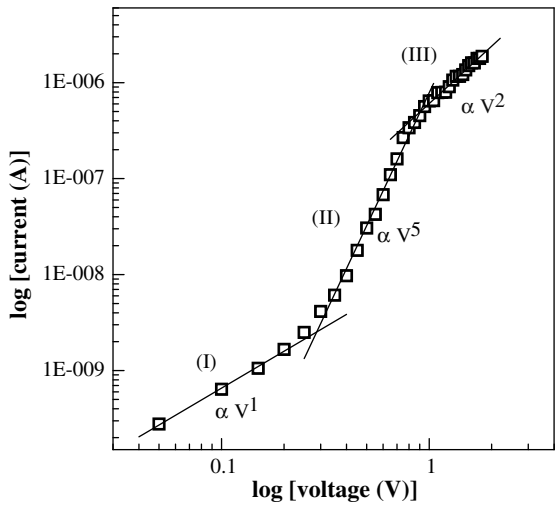

Fig. 4. The forward bias log(*J*) vs. log(*V*) plot of the Al/OG/*n*-Si/AuSb contact from the data in Fig. 3.

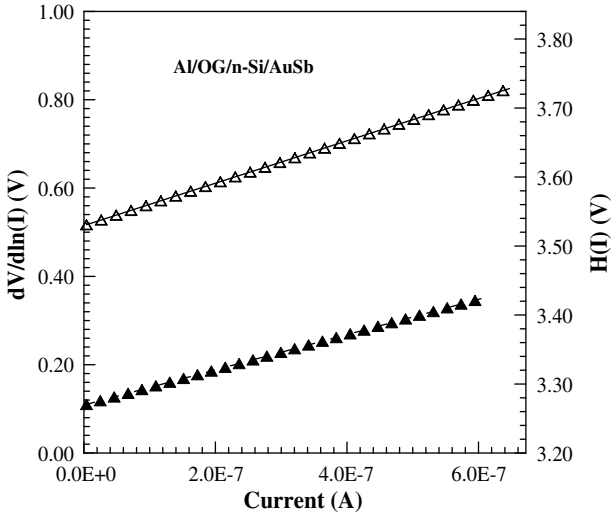

Fig. 5. A plot of $\frac{dV}{d(\ln I)}$ vs. *I* and H(I) vs. *I* obtained from forward bias current–voltage characteristics of the Al/OG/*n*-Si/AuSb structure.

Once the minimum of the F vs. V plot is determined, the value of barrier height can be obtained from Eq. (10), where $F(V_0)$ is the minimum point of $F(V)$, and V_0 is the corresponding voltage

$$\Phi_b = F(V_0) + \frac{V_0}{\gamma} - \frac{kT}{q} \tag{10}$$

Fig. 6 shows the $F(V)$–V plots of the junction. The value of the series resistance has been obtained from Norde's method for Al/OG/n-Si/AuSb junction. From Norde's functions R_s value is determined as:

$$R_s = \frac{kT(\gamma - n)}{qI} \tag{11}$$

From the F–V plot, the some parameters of the structure have been determined as Φ_b = 1.02 eV, R_s = 154.3 kΩ. There is a good agreement the values of R_s obtained from the forward bias ln$I$–V, Cheung functions and Norde functions.

The values of series resistance obtained from both methods are different from each other. Cheung functions are only applied to the non-linear region (high voltage region) of the forward bias ln$I$–V characteristics, while Norde's functions are applied to the full forward bias region of the ln$I$–V characteristics of the junctions. The value of series resistance may also be very high for the higher ideality factor values. The value of series resistance is very high, and this indicates that the series resistance is a current-limiting factor for this structure. The effect of the series resistance is usually modeled with series combination of a diode and a resistance R_s. The voltage across the diode can be expressed in terms of the total voltage drop across the diode and the resistance R_s. The very high series resistance behavior may be ascribed to decrease of the exponentially increasing rate in current due to space–charge injection into the OG thin film at higher forward bias voltage. Furthermore, Norde's model may not suitable method especially for the high ideality factor of the rectifying junctions, which non-agree with pure thermionic emission theory. We assume that another mechanism starts to control the current flow. This mechanism is with very high probability tunneling. Because, the tunneling process is important especially for a thin interfacial layer. This is probably only valid for determination of the values of series resistance.

Capacitance measurement is one of the most important nondestructive methods for obtaining information on rectifying contacts interfaces. In some contacts the capacitance under forward bias is larger than the space–charge capacitance predicted by basic theory. The difference between the measured and the space-charge capacitance is called the excess capacitance, and is attributed to interface states. The interface states can be created by crystal lattice discontinuities (dangling bonds), interdiffusion of atoms or a large density of crystal lattice defects close to the metal/semiconductor interface [15] or organic materials/semiconductor interface.

The C–V measurements of the structure were carried out at 10 kHz and 500 kHz frequencies. Differential capacitance measurements on a Schottky barrier measure the response of the barrier to an alternating voltage (a.c) superposed on a direct current (d.c) voltage. When the d.c. voltage corresponds to a reverse bias, the differential capacitance represents the response of the depletion layer to the a.c. signal. Fig. 7 shows the forward and reverse bias C–V characteristics of the structure measured at 10 kHz and f = 500 kHz frequency, at room temperature. The value of the capacitance is increasing in forward bias till a point where it reaches a maximum value, and decreases sharply after that. Measurement of the depletion region capacitance under forward bias is difficult because the diode is conducting and the capacitance is shunted by a large conductance. However, the capacitance can be easily measured as a function of the reverse bias [28]. The inset in Fig. 7 depicts C^{-2}–V plot from C–V data of the Al/OG/n-Si/AuSb device at 500 kHz. The non-linearity shown in the inset in Fig. 7 that indicates a non-uniform dopant density profile is ascribed to the interface states introduced by the native oxide layer plus OG organic layer and the surface irregularities/defects that cause the variation of the effective area. Assuming dielectric constant $\varepsilon_s = 11.9\varepsilon_0$, the approximate carrier concentration of n-Si is about 5×10^{17} cm^{-3}. The voltage axis intercept of the C^{-2}–V plot gives a value of about 0.76 V for diffusion voltage, V_d. Also, Schottky barrier has been obtained as 0.85 eV.

The junction capacitance is measured as a function of frequency and voltage. The capacitance–frequency (C–f) measurements of this structure were carried out at the various biases (0.00 V, +0.4 V and −0.4 V). These plots are seen at Fig. 8. As shown in this figure, the values of the measured capacitance are become almost constant up to the certain frequency value. Besides, the higher values of capacitance at low frequency are due to the excess capacitance resulting from the interface states in equilibrium with the n-Si that can follow the alternating current signal. Namely, the interface states at lower frequencies follow the alternating current signal, while at higher frequencies they cannot follow the alternat-

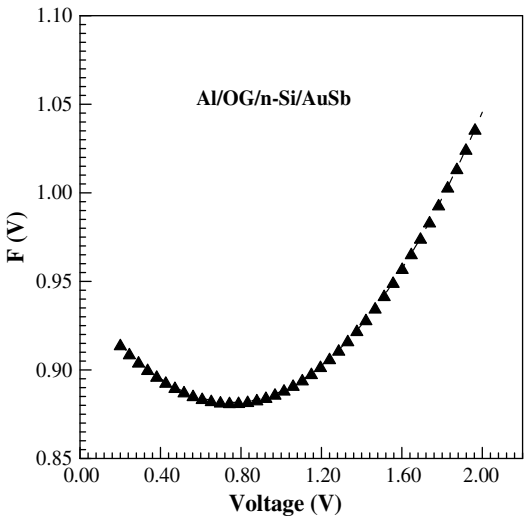

Fig. 6. $F(V)$ vs. V plot of the Al/OG/n-Si/AuSb structure.

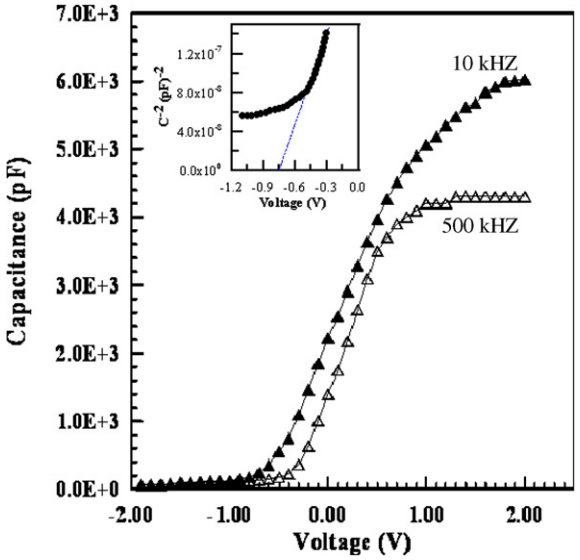

Fig. 7. The forward and reverse bias C–V characteristics of the Al/OG/n-Si/AuSb structure at 10 kHz and 500 kHz frequencies. Inset shows the reverse bias C^{-2}–V characteristic of the device at 500 kHz.

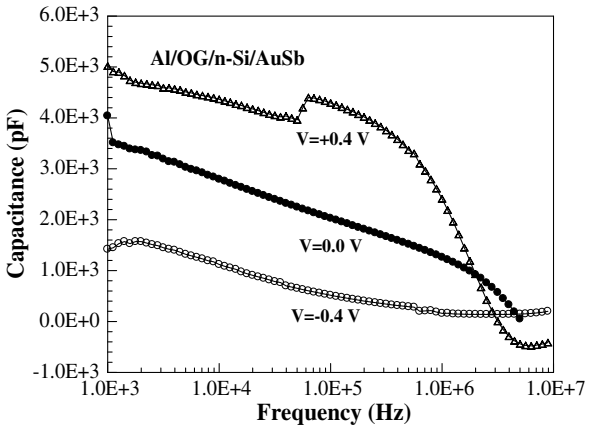

Fig. 8. The forward bias *C–f* characteristics of the Al/OG/*n*-Si/AuSb structure at various voltages.

ing current signal. The values of the capacitance at the high frequency region are only space-charge capacitance.

The voltage and frequency dependences of the junction capacitance are due to the particular features of a Schottky barrier, impurity level, high series resistance, etc. At low frequency, the capacitance measured is dominated by the depletion capacitance of the Schottky diode, which is bias-dependent and frequency-independent. As the frequency is increased, the total diode capacitance is affected not only by the depletion capacitance, but also by the bulk resistance and the dispersion capacitance, which is frequency-dependent and associated with hole or electron emission from slowly responding deep impurity levels [15].

In organic/inorganic semiconductor contact applications, in order to keep the technological difficulties and unknowns to a minimum, silicon is generally chosen as the substrate semiconducting material. In this structure, deposition of organic materials on the inorganic semiconductor can generate large number of interface states at the semiconductor surface that strongly influence the properties of the Al/OG/*n*-Si/AuSb structure. When these structures are considered as Schottky diodes, the devices comprise a high-resistivity layer (the depletion layer) in series with a low-resistivity layer, which has its own capacitance and resistance. In addition, the native oxide layer, which occurred at the right time in the cleaning procedure, between OG and *n*-Si can affect the capacitance.

4. Conclusions

In summary, we have investigated the *I–V, C–V* and *C–f* characteristics of the Al/OG/*n*-Si/AuSb structure. The values of the ideality factor, series resistance and barrier height obtained from two methods were compared. The downward concave curvature of the forward bias current-voltage characteristics at sufficiently large voltages is caused by the presence of the effect of series resistance. Thus, the concavity of the forward bias current–voltage characteristics increases with increasing series resistance value. The high resistance values have given the high ideality factors. Besides, the higher values of capacitance at low frequencies were attributed to the excess capacitance resulting from the interface states in equilibrium with the *n*-Si that can follow the a.c. signal.

References

[1] J. Lei, W. Liang, C.J. Brumlik, C.R. Martin, Synth. Met. 47 (1992) 351.
[2] M. Willander, A. Assadi, C. Svensson, Synth. Met. 55–57 (1993) 4099.
[3] M.E. Aydin, A. Türüt, Microelectron. Eng. 84 (12) (2007) 2875.
[4] O. Gullu, A. Turut, S. Asubay, J. Phys.: Condens. Matter 20 (2008) 045215.
[5] M. Zhu, T.H. Cui, K. Varahramyan, Microelectron. Eng. 75 (3) (2004) 269.
[6] G. Lloyd, M. Raja, I. Sellers, N. Sedghi, R. Di Lucrezia, S. Higgins, B. Eccleston, Microelectron. Eng. 59 (1–4) (2001) 323.
[7] S.A. Moiz, M.M. Ahmed, K.S. Karimov, ETRI J. 27 (3) (2005) 319.
[8] M.C. Petty, M. Bryce, An Introduction to Molecular Electronics, Oxford University Press, New York, 1995.
[9] J. Jortner, M.A. Ratner, Molecular Electronics, American Chemical Society, Washington DC, 1997.
[10] M.E. Aydin, F. Yakuphanoglu, J.H. Eom, D.H. Hwang, Physica B 387 (2007) 239.
[11] R.K. Gupta, R.A. Singh, Mater. Sci. Semicond. Process. 7 (2004) 83–87.
[12] O. Gullu, M. Cankaya, M. Biber, A. Turut, J. Phys.: Condens. Matter 20 (2008) 215210.
[13] O. Gullu, O. Baris, M. Biber, A. Turut, Appl. Surf. Sci. 254 (2008) 3039.
[14] T. Maeda, S. Takagi, T. Ohnishi, M. Lippmaa, Mater. Sci. Semicond. Process. 9 (2006) 706–710.
[15] E.H. Rhoderick, R.H. Williams, Metal–Semiconductor Contacts, second ed., Oxford, Clarendon, 1988.
[16] I.H. Campbell, S. Rubin, T.A. Zawodzinski, J.D. Kress, R.L. Martin, D.L. Smith, N.N. Barashkov, J.P. Ferraris, Phys. Rev. B 54 (20) (1996) 14321.
[17] M.D. Migahed, T. Fahmy, M. Ishra, A. Barakat, Polym. Test. 23 (2004) 361.
[18] T. Yamamoto, H. Wakayama, T. Fukuda, T. Kanbara, J. Phys. Chem. 96 (1992) 8677;
T. Yamamoto, T. Kanbara, C. Mori, H. Wakayama, T. Fukuda, T. Inone, S. Sasaki, J. Phys. Chem. 100 (1996) 12631.
[19] S.M. El-Sayed, H.M.A. Hamid, R.M. Radwan, Radiat. Phys. Chem. 69 (4) (2004) 339.
[20] M.G. Kang, H.H. Park, Vacuum 67 (1) (2002) 91.
[21] V.C. Nguyen, K.P. Kamloth, J. Phys. D: Appl. Phys. 33 (2000) 2230.
[22] M.M. El-Nahass, K.F. Abd-El-Rahman, A.A.M. Farag, A.A.A. Darwish, Organ. Electron. 6 (2005) 129.
[23] S. Aydogan, M. Saglam, A. Turut, Vacuum 77 (2005) 269;
S. Aydogan, M. Saglam, A. Turut, Polymer 46 (2005) 563.
[24] I.E. Vermeir, N.Y. Kim, P.E. Laibinis, Appl. Phys. Lett. 74 (1999) 3860.
[25] I. Musa, W. Eccleston, Thin Solid Films 343–344 (1999) 469.
[26] M. Cakar, C. Temirci, A. Turut, Synth. Met. 142 (2004) 177.
[27] A.R.V. Roberts, D.A. Evans, Appl. Phys. Lett. 86 (2005) 072105.
[28] S. Karatas, A. Turut, Vacuum 74 (1) (2004) 45.
[29] H.A. Cetinkara, A. Turut, D.M. Zengin, S. Erel, Appl. Surf. Sci. 207 (2003) 190.
[30] M.E. Aydin, A. Türüt, Microelectron. Eng. 84 (2007) 2875.
[31] S.M. El-Sayed, H.M.A. Hamid, R.M. Radwan, Radiat. Phys. Chem. 69 (2004) 339.
[32] S.R. Forrest, Chem. Rev. 97 (1997) 1793.
[33] T. Ben Jomaa, L. Beji, A. Ltaeif, A. Bouazizi, Mater. Sci. Eng. C 26 (2006) 530.
[34] S. Aydogan, M. Saglam, A. Turut, Microelectron. Eng. 85 (2008) 278.
[35] A. Turut, M. Saglam, H. Efeoglu, N. Yalcin, M. Yildirim, B. Abay, Physica B 205 (1995) 41.
[36] S.K. Cheung, N.W. Cheung, Appl. Phys. Lett. 49 (1986) 85.
[37] T. Kilicoglu, Thin Solid Films 516 (2008) 967.
[38] H. Norde, J. Appl. Phys. 50 (1979) 5052.
[39] S. Karatas, S. Altindal, A. Turut, M. Cakar, Physica B 392 (1–2) (2007) 43.